ACS APPLIED ELECTRONIC MATERIALS

pubs.acs.org/acsaelm

Article

Enhancement of Magnetic Stability in Antiferromagnetic CoO Films by Adsorption of Organic Molecules

Luca Gnoli,* Mattia Benini, Corrado Del Conte, Alberto Riminucci, Rajib K. Rakshit, Manju Singh, Samuele Sanna, Roshni Yadav, Ko-Wei Lin, Alessio Mezzi, Simona Achilli, Elena Molteni, Marco Marino, Guido Fratesi, Valentin Dediu, and Ilaria Bergenti

Cite This: *ACS Appl. Electron. Mater.* 2024, 6, 3138−3146

Read Online

ACCESS | Metrics & More | Article Recommendations | Supporting Information

ABSTRACT: Antiferromagnets are a class of magnetic materials of great interest in spintronic devices because of their stability and ultrafast dynamics. When interfaced with an organic molecular layer, antiferromagnetic (AF) films are expected to form a spinterface that can allow fine control of specific AF properties. In this paper, we investigate spinterface effects on CoO, an AF oxide. To access the magnetic state of the antiferromagnet, we couple it to a ferromagnetic Co film via an exchange bias (EB) effect. In this way, the formation of a spinterface is detected through changes induced on the CoO/Co EB system. We demonstrate that C_{60} and Gaq_3 adsorption on CoO shifts its blocking temperature; in turn, an increase in both the EB fields and the coercivities is observed on the EB-coupled Co layer. Ab initio calculations for the CoO/C_{60} interface indicate that the molecular adsorption is responsible for a charge redistribution on the CoO layer that alters the occupation of the d orbitals of Co atoms and, to a smaller extent, the p orbitals of oxygen. As a result, the AF coupling between Co atoms in the CoO is enhanced. Considering the granular nature of CoO, a larger AF stability upon molecular adsorption is then associated with a larger number of AF grains that are stable upon reversal of the Co layer.

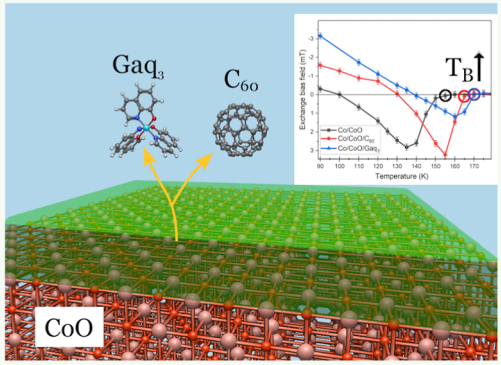

KEYWORDS: *antiferromagnets, hybrid interface, spinterface, molecular spintronics, organic spintronics, magnetic properties*

1. INTRODUCTION

The interface between organic molecules and a magnetic layer is considered to be the key element in defining the spin functionality of hybrid molecular spintronic devices.[1,2] Since the proposal in 2010 of interfacial spin-hybridization-induced polarized states as the main factors that control the spin and magnitude of the spin current injected in a molecular spintronic device,[3] several investigations focused on the formation of this so-called spinterface, a specific organic-magnet interface that can exploit spin-dependent effects. The spinterface formation affects the spin properties of both interface components. For example, it is responsible for the generation of spin polarization in the molecules[4,5] and for the change of the magnetic behavior of the ferromagnetic (FM) layer.[6,7] An emblematic example is provided by the adsorption of buckminster fullerene molecule (C_{60}) onto a cobalt (Co) layer:[7] as a result of hybridization between metallic d_z^2 and carbon p_z orbitals, the Co layer acquires an out-of-plane interfacial anisotropy that is able to give rise to a spin reorientation transition from in-plane to out-of-plane magnetization. Hybridization effects have been widely investigated both theoretically and experimentally considering FM metallic layers[8−10] while the adsorption and coupling of molecules on oxide surfaces with antiferromagnetic (AF) order have not been elucidated yet.[11−13] The investigation of such effects on systems featuring complex spin configurations allows thus to enrich our fundamental knowledge of spinterfaces and also to explore the possibility of tuning with molecules some intrinsic AF properties such as ultra-fast magnetization dynamics[14] and magnon-mediated spin transport.[15] In this view, because of the insensitivity of AF to the external magnetic field and with the aim of evidencing the effect of coupling between AF and organics, we have considered the AF layer also coupled to an FM featuring thus an exchange bias (EB) effect. This effect manifests as a shift of the magnetic hysteresis loop along the field axis after field cooling the sample below the Néel temperature (T_N) of the AF. The selected AF is cobalt oxide (CoO) since its properties are well known and the Co/CoO interface is considered a model system for such investigations.[16]

Received: November 13, 2023
Revised: February 14, 2024
Accepted: February 19, 2024
Published: May 10, 2024

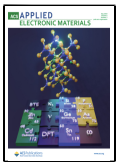

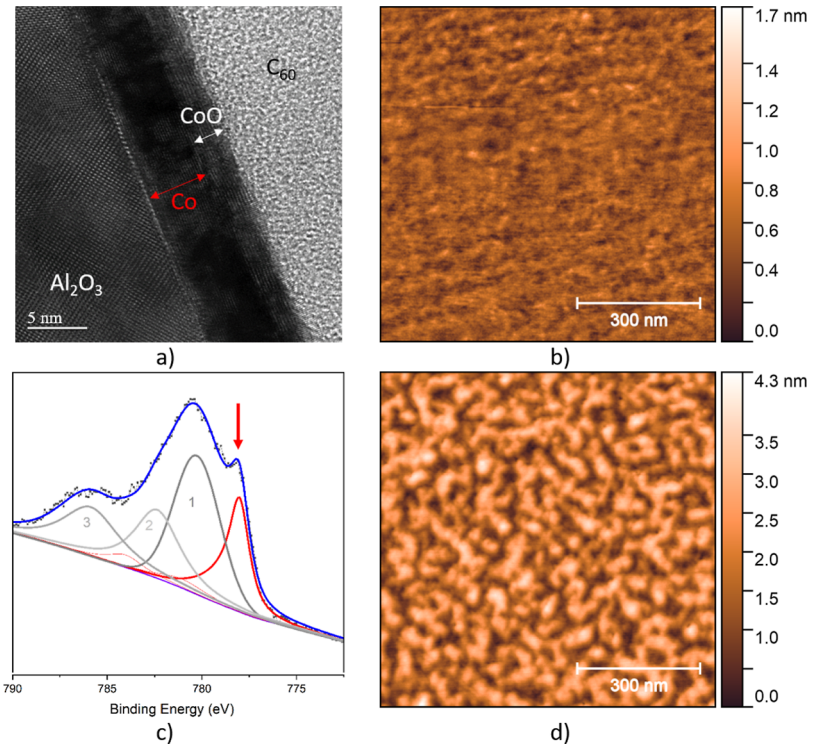

Figure 1. a) Cross-sectional TEM images of Co/CoO/C_{60} deposited on Al_2O_3 substrate, (b) AFM images of bare CoO surface, (c) XPS spectra of Co 2p region and the spectral deconvolution of Co $2p_{3/2}$, arrow indicates the metallic Co contribution. (d) AFM images of 25 nm Gaq_3 on CoO.

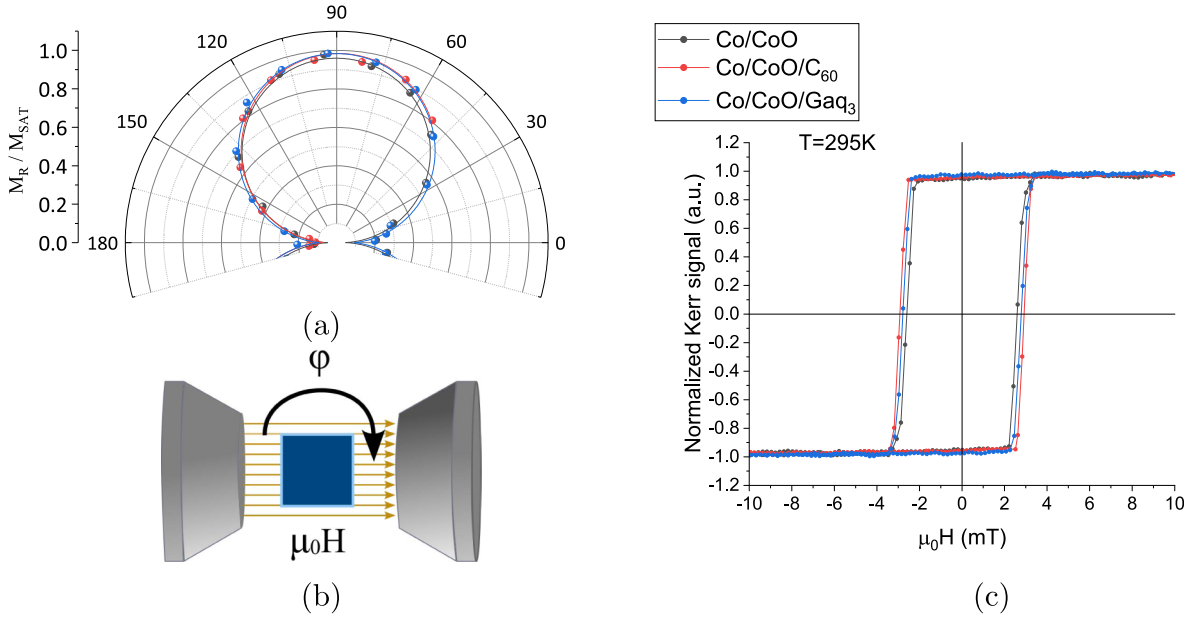

Figure 2. a) Polar graphical representation of normalized remanence obtained from MOKE hysteresis curves acquired at different azimuthal angles at RT. (b) Representation of the measurement setup employed for in-plane anisotropy study. (c) Hysteresis cycles corresponding to the easy axis direction.

2. RESULTS AND DISCUSSION

The Co/CoO exchange-biased bilayers were prepared in UHV conditions with subsequently controlled oxidations starting from a Co film of 7 nm as reported in detail in Section 4. The samples were produced in a single run with exactly the same Co/CoO thickness. On top of the two samples, the organic layer was deposited by means of shadow masking techniques allowing exactly the same preparation conditions but a different organic overlayer. As organic materials, we considered two molecules that are known to generate a spinterface with FM layers: the tris(8-hydroxyquinoline) gallium (Gaq_3)[17] and the buckminsterfullerene (C_{60}).[18] We start from the assessment of chemical, structural, and morphological properties of the Co/CoO exchange-biased bilayer. Figure 1a shows a typical cross-sectional image of a Co/CoO bilayer covered by a C_{60} organic layer. A clear interface between the Co film and the Al_2O_3 substrate is observed. Layers are continuous and a

https://doi.org/10.1021/acsaelm.3c01599
ACS Appl. Electron. Mater. 2024, 6, 3138−3146

remarkable crystalline order of CoO is visible, but it is worth noting that, in some regions, the oxide layer is jagged and penetrates into the Co layer. The average thickness of the Co film is estimated at 5.1 nm, and that of the oxide layer is estimated at 2.8 nm. The corresponding fast Fourier transform analysis indicates that Co and CoO are crystalline with an FCC structure. AFM measurements of the CoO surface indicate a root-mean-square roughness of about 0.3 nm over an area of 1 × 1 μm^2 at the surface (see Figure 1b). As the oxidation was performed at room temperature, the formed cobalt oxide is assumed to be CoO.[19] XPS was employed to confirm the chemical nature of the oxide layer. The Co $2p_{3/2}$ peak is dominated by the distinctive components associated with the cobalt monoxide (Co(II)) at BE(1) = 780.3 eV, BE(2) = 782.4 eV, BE(3) 785.8 eV[20] with a sharp shoulder at BE = 778.1 eV associated with the metallic Co layer underneath.

The XPS spectra line shape confirms that the predominant oxide species is the cobalt monoxide.[20] The 25 nm thick organic layer completely covers the CoO surface, thus maximizing the CoO/organic interaction as evidenced by both TEM measurements for C_{60} and AFM for Gaq_3. The deposition of the organic molecule increases the surface roughness reaching the values of 0.7 nm for C_{60} and 1.2 nm for Gaq_3 (Figure 1d) both values comparable with the molecule dimension.

We move to the magnetic characterization of samples with the aim of investigating the effects of the organic molecules. Longitudinal MOKE measurements performed at 295 K, i.e., above the nominal bulk Néel temperature $T_N \sim 291$ K of the CoO, with the applied magnetic field at various azimuthal angles ϕ with respect to the sample orientation in the configuration shown in Figure 2b, evidence the presence of an in-plane uniaxial anisotropy for Co layer as shown in Figure 2a and evidenced in previous studies for the same growth conditions.[6] The hysteresis loops shown in Figure 2c of the Co layers do not present any EB effect, as expected at temperatures above the T_N. Moreover, all samples have similar coercive fields at 295 K within the error range of 3 Oe.

The temperature-dependent magnetic characterization has been carried out with a magnetic field applied along the Co easy axis direction. The AF state is set by a field cooling procedure by applying H = 75 mT from 300 K down to 80 K. Figure 3 shows the typical hysteresis loops collected at 90 K featuring the EB effect.

As expected, the sign of H_{EB} is opposite the direction of the cooling field, making it easier to reverse the magnetization of the Co in the cooling field direction than in the opposite one. This phenomenon is known as negative EB. Training effect also appears in our samples, showing a reduction of H_{EB} magnitude in successive hysteresis loops until stability is reached.[21−23] The origin of the training effect is still debated[16] but it is often ascribed to the rearrangement of AF moments both at the frustrated FM/AF interface and in the bulk of the AF layer, upon the application of the first magnetic field cycle due both to athermal and thermal effects.[24−26]

Figure 4 shows the temperature dependence of both H_{EB} and H_C fields deduced from hysteresis cycles measured after the training process is completed, i.e., they do not show significant variation between consecutive loops. H_{EB} strength (Figure 4a) decreases linearly with increasing T starting from the lowest initial temperature up to the temperature where the value of the EB field changes sign. This temperature corresponds to the value in which a positive EB field is

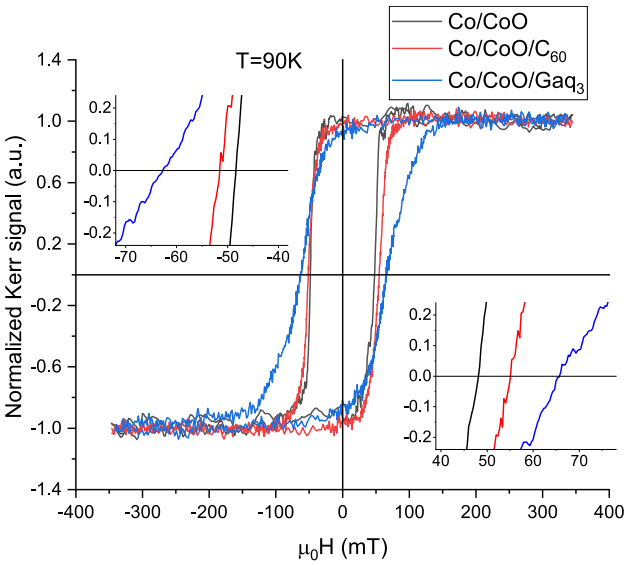

Figure 3. Hysteresis cycles measured at 90 K obtained after cooling in a magnetic field of 75 mT. The reported cycles refer to the three samples after the training of the AF layer is completed.

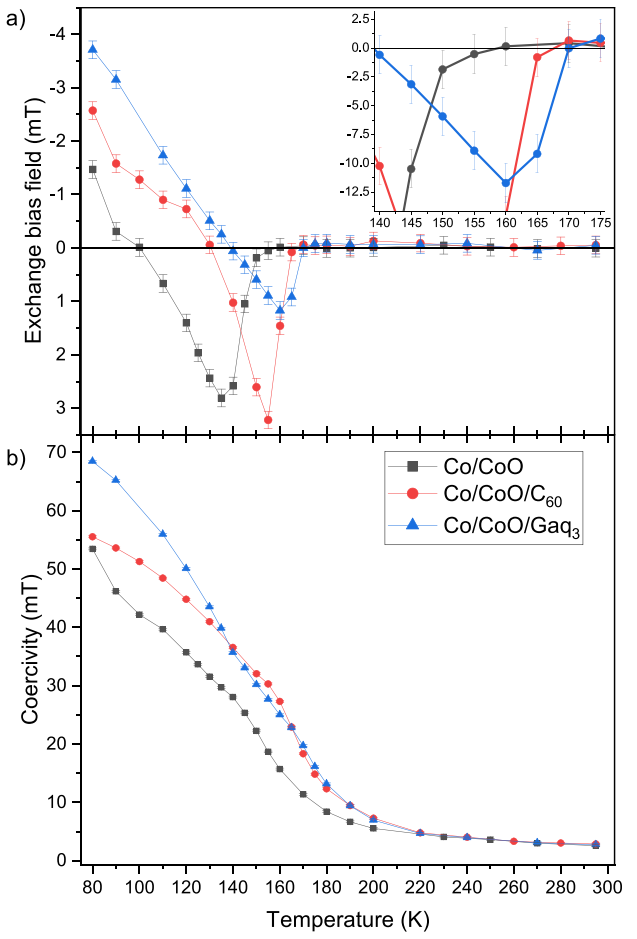

Figure 4. Temperature evolution of (a) EB field and (b) coercivity of the samples. The three samples have been cooled from 300 K to 80 K with a field of 75 mT.

registered and will be referred to as the positive EB temperature (T_P). The T_P value varies for all three samples as shown in Table 1. The lower T_P is registered for CoO,

https://doi.org/10.1021/acsaelm.3c01599
ACS Appl. Electron. Mater. 2024, 6, 3138−3146

Table 1. Positive Exchange Bias and Blocking Temperatures for all the Three Samples

sample	T_P	T_B
Co/CoO	100 ± 10 K	155 ± 5 K
Co/CoO/C_{60}	125 ± 10 K	165 ± 5K
Co/CoO/Gaq_3	140 ± 10 K	170 ± 5K

followed by the sample covered with C_{60} and finally the one covered with Gaq_3. Moving toward higher temperatures, H_{EB} reaches its maximum positive value and then approaches zero at a temperature referred to as the blocking temperature (T_B). The lowest T_B value is obtained for the CoO bare sample. Higher T_B values are obtained in the presence of C_{60} and Gaq_3, resembling the order registered for T_P.

The appearance of positive EB has been observed in Co/CoO bilayers both in epitaxial[27] and polycrystalline forms.[22,28,29] The intensity of positive EB and the temperature T_P depend on the FC strength as shown in the Supporting Information and it can be explained in terms of a competition between bulk and interface magnetic ordering in the AF occurring when a significant fraction of the AF uncompensated magnetization follows the FM reversal.[27,29]

Also, the dependency of H_C on temperature, shown in Figure 4b, clearly shows the effect of the interaction with the molecular layer. Looking at the evolution of H_C in the three samples, we can identify four temperature ranges. The first and highest one corresponds to temperatures at which the AF is expected to have almost completely lost its order and stability not influencing anymore the Co: H_C does not show any appreciable difference between samples. Moving toward lower temperatures, at about 200 K, CoO covered with C_{60} and Gaq_3 shows a significant change with respect to the bare CoO. In this region, the effect of the AF layer is already detected. At temperatures higher than the blocking temperature, the increase in coercivity can be attributed to a partial order in the AF able to influence the rotation of Co magnetization but not strong enough to produce any visible shift of the hysteresis cycle.[16,30]

In the region corresponding to the maximum positive EB, each sample presents a hump in the H_C temperature dependence and, for temperatures below T_B, the H_C increases. In addition, moving toward the lowest investigated temperatures for both Gaq_3 and C_{60}, H_C reduces its growth rate, indicating that the AF moment configuration remains essentially unchanged during FM moment reversal.[31] We cannot exclude a similar trend also for bare Co/CoO but at temperatures lower than the investigated ones. The higher blocking temperatures and EB values in samples with molecular layers indicate that the presence of organic molecules at the interface with AF generates an increased AF stability over a wider temperature range.

The ability of organic molecules to modify magnetic states has been tested both theoretically[32,33] and experimentally[6,7] on FM layers thanks to the hybridization between the d orbitals of the FM and the π orbitals of the molecules. Such orbital redistribution impacts both the exchange interaction and the magnetic anisotropy energy producing an increase in the Curie temperature as well as of the magnetic coercivity fields.[32] To elucidate the specific features of the coupling with the AF layer, we investigated by means of density functional theory (DFT) the adsorption of C_{60} molecules on CoO(001) in a high-density packing arrangement, as described in Section 4.

Nine possible adsorption configurations (see Figure S2 in the Supporting Information) are explored that differ for the orientation of the molecule with respect to the substrate (facing with a pentagon, hexagon, bond) and the adsorption site of the molecule (on Co, on O, on bridge site between Co rows). The most stable configuration is obtained with a hexagonal face adsorbed on an oxygen atom as shown in Figure 5 (adsorption energy equal to $E = -3.92$ eV). For this

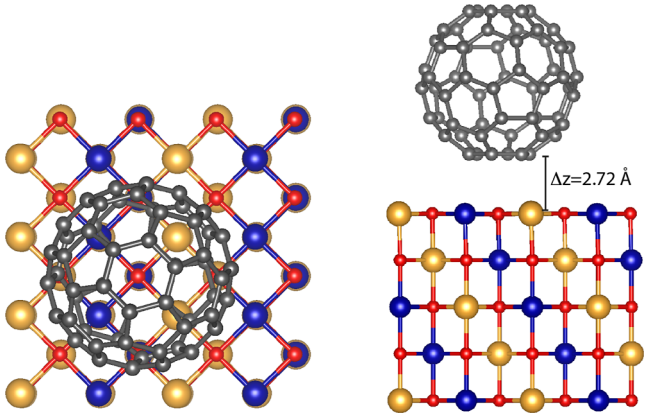

Figure 5. Top and lateral view of the most stable adsorbed configuration. Blue/yellow atoms correspond to Co with a different spin forming the AF structure. Red and gray atoms are oxygen and carbon, respectively.

orientation of the molecule and adsorption site, we considered also a rotation of 30° that nevertheless makes the system less stable (Figure S2). The C_{60}−CoO distance is 2.72 Å.

The interaction between the C_{60} and the CoO surface is responsible for a transfer of electrons toward the molecule accompanied by a charge redistribution in the surface layer of CoO (see Figure 6a,b and details in the Supporting Information). Such charge transfer is responsible for a tiny variation of the magnetic moments of the Co atoms and a small induced magnetic moment mostly localized on the C atoms facing the surface (Figure 6c,d). One-half of the total magnetic moment is localized on the six atoms of the adsorbing hexagon, with atomic magnetic moments ranging between +0.02 μ_B and −0.02 μ_B. The carbon atoms in the hexagon display an AF ordering. The overall net magnetic moment on the entire molecule is equal to 0.005 μ_B.

On the CoO surface, the absolute magnetic moment of antiparallel aligned Co atoms (noted as Co1 and Co2) is reduced with respect to the bulk; see Figure 6d in which the difference with respect to the bare CoO surface is shown (positive values correspond to spin down Co2 atoms and negative ones to spin up Co1). This effect characterizes the whole Co surface atoms but it is enhanced in the four Co atoms just below the molecule. Although the induced changes in the spin polarization of oxygen atoms are negligible, they lead to a net-induced magnetic moment in the first layer (0.02 μ_B) that decays quickly down into the CoO. Accordingly, also the intralayer-induced net magnetic moment of Co atoms is smaller in deeper layers (see Figure S3 in the Supporting Information) so that the overall magnetic change arising at the interface with the molecules is almost completely vanished in the fourth and fifth layers.

Although the changes of magnetic properties induced by the interaction with C_{60} are mild and limited to the interface, we

https://doi.org/10.1021/acsaelm.3c01599
ACS Appl. Electron. Mater. 2024, 6, 3138−3146

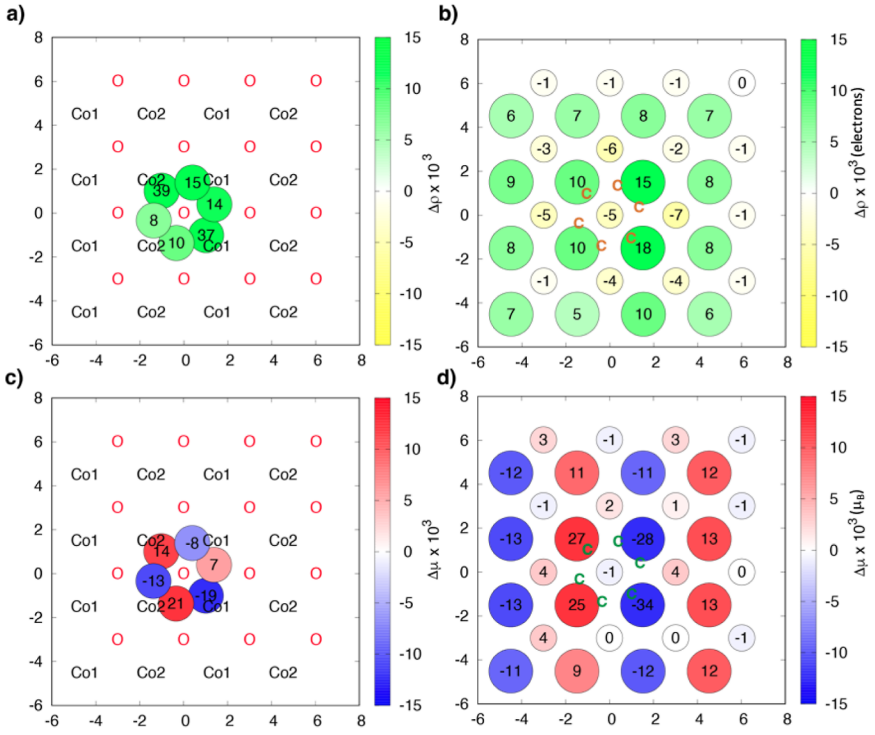

Figure 6. Induced charge (a,b) and spin (c,d) on selected planes parallel to the surface. Color scale reports the difference of charge and spin with respect to the clean CoO surface when C_{60} molecules are adsorbed. Panels (a,c) consider the plotted quantities onto a plane passing through the lowermost hexagonal face of the molecule, near the surface. (b,d) Refer to a plane passing through the surface layer. Labels Co1 and Co2 in (a,c) mark the position of Co atoms of the substrate with opposite magnetization and correspond to the large circle in panel (b,d), where O atoms are instead reported as a small circle. The labels on atoms report the values of induced charge and spin, according to the color scale.

observe an overall charge redistribution in the CoO oxide layer which alters the occupation of the d orbitals of Co atoms and of the p orbitals of oxygen to a minor extent. The minority spin projected density of states (PDOS) of the surface layer, reported in Figure 7 together with the PDOS of the clean CoO surface, evidence the changes of the Co d orbitals due to the interaction with molecular states (energy position of HOMO − 1, HOMO, LUMO, LUMO + 1 are reported with blue tics, C_{60} PDOS in the Supporting Information). The integral of the occupied PDOS (values for pristine and covered CoO reported in black and red in Figure 7) reveals an increase in the electronic charge of d_{xz} orbitals, which is mainly due to the interaction with the HOMO and HOMO − 1 state of the molecule. Conversely, the LUMO state lies in the energy gap of CoO/C_{60}, while the LUMO + 1 hybridizes with unoccupied d orbitals except the d_{yz}. Upon the adsorption of C_{60}, we observe a depletion of $d_{x^2-y^2}$ states and a mild filling of d_{xy} states. This effect is expected to modify the superexchange being associated with a change of the electronic density around Co atoms with respect to the surrounding oxygen atoms.

The variations in the average occupations of the Co orbitals affect all the layers in the slab and may be then related to the change of the magnetic coupling in the CoO film.

To evaluate the impact of the orbital occupations on the AF state, we have performed calculations for different spin configurations of the CoO(001) surface with and without adsorbed molecules to extract the exchange coupling in the oxide layer. The geometry of the various spin configurations was kept fixed to the ground state to exclusively account for the effect of the spin-flip on the total energy of the molecules. By exploiting a Heisenberg model for the magnetic interaction in the Hamiltonian, we are able to estimate the changes in the strength of the AF order when the molecules are deposited on the surface. The AF order is indeed due to a superexchange interaction between Co spins with coupling parameter J, mediated by oxygen atoms. This one represents the strongest among the Co−Co interactions, being the one not mediated by oxygen almost negligible.[34,35] The value of J is derived from a system of equations $E_k = \sum_{<i,j>} J_{i,j} S_{k,i} S_{k,j}$ in which the sum on indexes $<i,j>$ is done on unique next nearest neighbor Co pairs, E_k is the total energy of the spin configuration k (with arbitrary reference) and $S_{k,i}$, $S_{k,j}$ are the spin directions associated with Co atoms and they are set equal to +1 or −1. To set a system of equations from which to extract J, we consider different spin configurations in which the spin of a single Co atom on the surface is flipped. The obtained exchange coupling parameter J has an average value (mediated on the surface Co atoms) of −21 meV that increases to −27 meV for CoO/C_{60}.

The evaluation of the critical temperature cannot be extracted directly from these calculations, preventing any quantitative comparison with the change of the blocking temperature deduced experimentally. The thermal stability of AF is a key ingredient for the modeling of polycrystalline exchange-biased layers as described originally by Fulcomer and Charap[36] and others.[30,37] We stress that the Co/CoO under investigation in this paper presents a granular structure, as evidenced by the TEM characterization in Figure 1. In the simplest description, a polycrystalline AF layer can be modeled by a granular domain structure in which the grains are weakly interacting entities and the energy barrier that is opposed to thermal fluctuations depends directly on the volumes of the single grains.[30,37] Following those models, the EB effect is directly proportional to the number of grains with a volume big

https://doi.org/10.1021/acsaelm.3c01599
ACS Appl. Electron. Mater. 2024, 6, 3138−3146

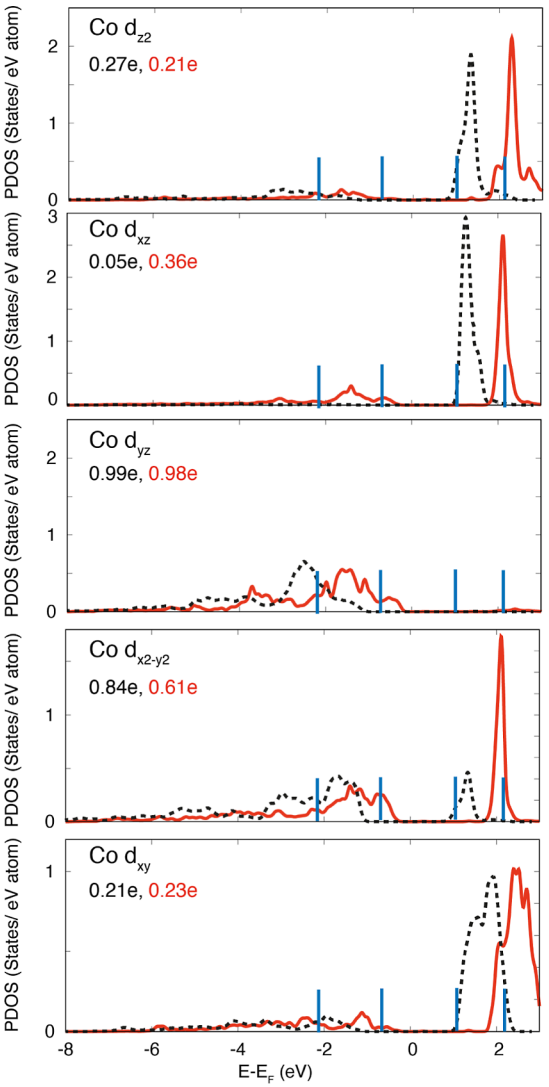

Figure 7. Minority spin density of states of surface Co projected on d orbitals for the C_{60}/CoO (red) and the clean CoO surface (black). The electronic occupation of the orbitals is reported with the same color code. The position of molecular states near the Fermi level is marked with blue tics.

enough to remain pinned during the FM reversal. We can then consider a volume distribution as shown in Figure 8 where $f(V)$ represents the volume density distribution of domains of the AF layer. It is then possible to identify a critical volume V_c of domains below which the AF domain is not stable enough and reverses following the FM layer, while domains with a larger volume maintain the AF state stable. In this scenario, the effect of increased AF stability of the CoO upon molecule adsorption is then analogous to a decrease in V_c, producing an increase in the number of grains with a stable configuration as shown in Figure 8b.

3. CONCLUSIONS

In this paper, we have investigated the effect of the adsorption of organic molecules (Gaq_3 and C_{60}) on a polycrystalline CoO AF thin layer coupled by EB to an FM Co layer. In both cases, the molecular adsorption induces an increase of the blocking temperature of Co/CoO associated also with higher EB fields and higher coercivities. Ab initio calculations performed on the

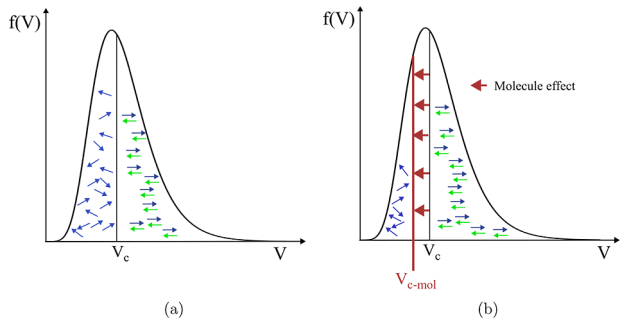

Figure 8. Schematic of the energy barriers to reversal, showing the critical volume V_c of AF grains below which the AF domains are thermally unstable and rotate with the FM layer (a). The increased stability of AF domains induced by molecular adsorption can be modeled as a decrease of the V_c, reducing the number of thermally unstable AF domains (b).

model CoO/C_{60} interface indicate a partial transfer of electrons toward the molecule accompanied by a charge redistribution in the surface layer of CoO. While the magnetic moments of the Co atoms are only slightly affected, the charge redistribution in the CoO oxide layer alters the occupation of the d orbitals of Co atoms inducing a more stable AF coupling in the surface of the CoO. Considering the granular structure of the Co/CoO bilayer under investigation, we refer to polycrystalline models and we associate the increased AF stability with the larger number of AF grains that remain pinned under FM switching, inducing an increase of H_{EB}.

4. EXPERIMENTAL/METHODS

4.1. Sample Preparation. The Co/CoO exchange-biased bilayers were prepared on single crystal Al_2O_3 (0001) substrates. A 7 nm thick Co film was deposited by means of e-beam evaporation in ultra-high vacuum (UHV) conditions under a base pressure of 10^{-10} mbar at room temperature. The AF CoO layer was obtained by oxidizing the Co layer in situ in the atmosphere of pure oxygen (purity 99.999%) with an exposure of 10^4 L. To obtain a thicker CoO layer, an additional Co layer of 1 nm was then deposited on top of the CoO and then oxidized with the same oxygen dose. Without breaking the vacuum, on top of the CoO layer, a 25 nm thick organic layer was deposited. The deposited organic materials are Gaq_3[17] and C_{60}.[18] The materials were thermally evaporated respectively at 255 and 360 °C at a base pressure of 1×10^{-8} mbar. The investigated samples were produced in a single run with exactly the same Co/CoO thickness.

4.2. Transmission Electron Microscopy (TEM). TEM was performed using a JEOL (JEM-2100F) instrument operating at 200 kV. Cross-sectional samples were prepared using standard "lift-out" procedures on a JEOL (JIB-4601F) focused ion beam system and were typically polished to a ~100 nm thickness: further thinning tends to damage the delicate organic layer.

4.3. Atomic Force Microscopy. The topography of the films was investigated using an AFM Smena microscope (NT-MDT, Moscow, Russia) in intermittent contact mode under ambient conditions.

4.4. X-ray Photoelectron Spectroscopy (XPS). XPS measurements were carried out using an ESCALAB 250Xi spectrometer (Thermo Fisher Scientific, UK) equipped with a monochromatic Al K-α source and six channeltrons as the detection system. The apparatus works in a UHV system, where the base pressure of the analysis chamber during the experiments was approximately 10^{-10} mbar. The spectra were collected operating at constant pass energy CAE = 50 eV. The accuracy of the measurements was ±0.1 eV.

4.5. Magneto-Optical Kerr System. Magnetic hysteresis loop measurements were performed with a longitudinal magneto-optic Kerr effect system (λ_{exc} = 632.8 nm) equipped with a 50 kHz photoelastic modulator (HINDS) and with H_{max} = 4 kOe applied

https://doi.org/10.1021/acsaelm.3c01599
ACS Appl. Electron. Mater. 2024, 6, 3138−3146

magnetic field in the film plane. To induce the EB effect, samples were cooled in a static magnetic field and then hysteresis loop data were collected in the temperature range of 80−300 K. For each loop, the coercive (H_C) and EB fields (H_{EB}) were deduced. The quantities of H_{EB} and H_C are calculated as $H_{EB} = (H_{C1} + H_{C2})/2$ and $H_C = (|H_{C1}| + |H_{C2}|)/2$, where H_{C1} and H_{C2} denote the coercive fields at the descending and ascending branches of the hysteresis loop, respectively. The reset of the magnetic state of the CoO AF layer was obtained by heating the sample to 300 K, above the Néel temperature of bulk CoO (~291 K).[16]

4.6. Computational Model. Ab initio calculations were performed in DFT, exploiting the plane-wave pseudopotential scheme implemented in the PWSCF code of the Quantum ESPRESSO distribution.[38,39] We use the vdW-DF-c09 functional[40,41] and the scalar-relativistic ultrasoft pseudopotentials adopted in previous works (see ref 42 and references therein) and from the PS library database.[43] We adopt a Hubbard model for correlated electrons of Co in the rotationally invariant formalism of Dudarev. The effective U parameter has been set to 4 for Co. To reproduce the expected occupation of the t_{2g} d levels in the orthorhombic crystal field we set the initial occupations for the bulk Co atoms in the inner layers of the slab. Total energy calculations aimed to determine the adsorption energy and the most stable adsorption site of the molecule were performed for a slab including three layers of CoO(001) by relaxing the molecule and the external surface layer until forces reached a tolerance of 0.001 Ry/Bohr. Electronic and magnetic properties of the stable adsorbed configuration are calculated for a thicker slab with 5 atomic layers. The free vacuum space in the direction perpendicular to the slab amounts to 25 Å. We considered C_{60} molecules arranged with a periodicity determined by a square 2 × 4 supercell of CoO(001) including 16 Co atoms per layer. The energy cutoff for the wave function and the charge density were set equal to 45 and 270 Ry, respectively. A 4 × 4 × 1 k-mesh Monkhorst−Pack grid was used to sample the Brillouin zone.

■ ASSOCIATED CONTENT

Supporting Information

The Supporting Information is available free of charge at https://pubs.acs.org/doi/10.1021/acsaelm.3c01599.

Temperature dependency of coercivity and EB field with a 200 mT bias field cooling. Molecule adsorption details. Induced charge and magnetic moments distribution details. Further information on C_{60}/CoO PDOS (PDF)

■ AUTHOR INFORMATION

Corresponding Author

Luca Gnoli − *CNR ISMN, 40129 Bologna, Italy;* orcid.org/0000-0003-3749-6225; Email: luca.gnoli@ismn.cnr.it

Authors

Mattia Benini − *CNR ISMN, 40129 Bologna, Italy;* orcid.org/0000-0001-7568-9648

Corrado Del Conte − *Department of Physics and Astronomy "A. Righi", University of Bologna, I-40127 Bologna, Italy*

Alberto Riminucci − *CNR ISMN, 40129 Bologna, Italy;* orcid.org/0000-0003-0976-1810

Rajib K. Rakshit − *CNR ISMN, 40129 Bologna, Italy*

Manju Singh − *CNR ISMN, 40129 Bologna, Italy*

Samuele Sanna − *Department of Physics and Astronomy "A. Righi", University of Bologna, I-40127 Bologna, Italy*

Roshni Yadav − *Materials Science and Engineering Department, National Chung Hsing University, Taichung 402, Taiwan;* orcid.org/0000-0001-8107-3348

Ko-Wei Lin − *Materials Science and Engineering Department, National Chung Hsing University, Taichung 402, Taiwan*

Alessio Mezzi − *CNR ISMN, 00015 Monterotondo Scalo, Italy*

Simona Achilli − *Physics Department, Università degli Studi di Milano, 20133 Milan, Italy;* orcid.org/0000-0001-6812-5043

Elena Molteni − *Physics Department, Università degli Studi di Milano, 20133 Milan, Italy;* orcid.org/0000-0002-0153-5491

Marco Marino − *Physics Department, Università degli Studi di Milano, 20133 Milan, Italy*

Guido Fratesi − *Physics Department, Università degli Studi di Milano, 20133 Milan, Italy;* orcid.org/0000-0003-1077-7596

Valentin Dediu − *CNR ISMN, 40129 Bologna, Italy*

Ilaria Bergenti − *CNR ISMN, 40129 Bologna, Italy;* orcid.org/0000-0003-0628-9047

Complete contact information is available at: https://pubs.acs.org/10.1021/acsaelm.3c01599

Notes

The authors declare no competing financial interest.

■ ACKNOWLEDGMENTS

The authors acknowledge the support of the EC projects SINFONIA (H2020-FET-OPEN-964396) and INTERFAST (H2020-FET-OPEN-965046). The authors acknowledge Federico Bona for the technical support.

■ REFERENCES

(1) Cinchetti, M.; Dediu, V. A.; Hueso, L. E. Activating the molecular spinterface. *Nat. Mater.* **2017**, *16*, 507−515.

(2) Bergenti, I.; Dediu, V. Spinterface: A new platform for spintronics. *Nano Mater. Sci.* **2019**, *1*, 149−155.

(3) Barraud, C.; Seneor, P.; Mattana, R.; Fusil, S.; Bouzehouane, K.; Deranlot, C.; Graziosi, P.; Hueso, L.; Bergenti, I.; Dediu, V.; Petroff, F.; Fert, A. Unravelling the role of the interface for spin injection into organic semiconductors. *Nat. Phys.* **2010**, *6*, 615−620.

(4) Bergenti, I.; Kamiya, T.; Li, D.; Riminucci, A.; Graziosi, P.; MacLaren, D. A.; Rakshit, R. K.; Singh, M.; Benini, M.; Tada, H.; Smogunov, A.; Dediu, V. A. Spinterface Effects in Hybrid $La_{0.7}Sr_{0.3}MnO_3/SrTiO_3/C_{60}$/Co Magnetic Tunnel Junctions. *ACS Appl. Electron. Mater.* **2022**, *4*, 4273−4279.

(5) Djeghloul, F.; Gruber, M.; Urbain, E.; Xenioti, D.; Joly, L.; Boukari, S.; Arabski, J.; Bulou, H.; Scheurer, F.; Bertran, F.; Le Fèvre, P.; Taleb-Ibrahimi, A.; Wulfhekel, W.; Garreau, G.; Hajjar-Garreau, S.; Wetzel, P.; Alouani, M.; Beaurepaire, E.; Bowen, M.; Weber, W. High spin polarization at ferromagnetic metal−organic interfaces: a generic property. *J. Phys. Chem. Lett.* **2016**, *7*, 2310−2315.

(6) Benini, M.; Allodi, G.; Surpi, A.; Riminucci, A.; Lin, K.-W.; Sanna, S.; Dediu, V. A.; Bergenti, I. In-Depth NMR Investigation of the Magnetic Hardening in Co Thin Films Induced by the Interface with Molecular Layers. *Adv. Mater. Interfaces* **2022**, *9*, 2201394.

(7) Bairagi, K.; Bellec, A.; Repain, V.; Chacon, C.; Girard, Y.; Garreau, Y.; Lagoute, J.; Rousset, S.; Breitwieser, R.; Hu, Y.-C.; Chao, Y. C.; Pai, W. W.; Li, D.; Smogunov, A.; Barreteau, C. Tuning the Magnetic Anisotropy at a Molecule-Metal Interface. *Phys. Rev. Lett.* **2015**, *114*, 247203.

(8) Ngassam, F.; Urbain, E.; Joly, L.; Boukari, S.; Arabski, J.; Bertran, F.; Le Fèvre, P.; Garreau, G.; Wetzel, P.; Alouani, M.; Bowen, M.; Weber, W. Fluorinated Phthalocyanine Molecules on Ferromagnetic Cobalt: A Highly Polarized Spinterface. *J. Phys. Chem. C* **2019**, *123*, 26475−26480.

(9) Brambilla, A.; Picone, A.; Giannotti, D.; Calloni, A.; Berti, G.; Bussetti, G.; Achilli, S.; Fratesi, G.; Trioni, M. I.; Vinai, G.; Torelli, P.; Panaccione, G.; Duò, L.; Finazzi, M.; Ciccacci, F. Enhanced Magnetic

Hybridization of a Spinterface through Insertion of a Two-Dimensional Magnetic Oxide Layer. *Nano Lett.* **2017**, *17*, 7440−7446.
(10) Orlando, F.; Fratesi, G.; Onida, G.; Achilli, S. Tailoring the magnetic ordering of the Cr_4O_5/Fe(001) surface via a controlled adsorption of C_{60} organic molecules. *Phys. Chem. Chem. Phys.* **2021**, *23*, 7948−7954.
(11) Shao, Y.; Pang, R.; Pan, H.; Shi, X. Fullerene/layered antiferromagnetic reconstructed spinterface: Subsurface layer dominates molecular orbitals' spin-split and large induced magnetic moment. *J. Chem. Phys.* **2018**, *148*, 114704.
(12) Vasili, H. B.; Alotibi, S.; Valvidares, M.; Gargiani, P.; Rogers, M.; Ali, M.; Moorsom, T.; Burnell, G.; Hickey, B. J.; Cespedes, O. Spin Transport, Unidirectional Bias and the Effect of Molecular Interfaces in a Metallic Antiferromagnet. In *Proceeding of INTERMAG Conference*; 2023.
(13) Bergenti, I.; Riminucci, A.; Graziosi, P.; Albonetti, C.; Benini, M.; Toffanin, S.; Lopez, S. G.; Rakshit, R. K.; Singh, M.; Bentley, P. D.; Melchakova, I. A.; Avramov, P. V.; Dediu, V. A.; Pratt, A. Spinterface Formation at α-Sexithiophene/Ferromagnetic Conducting Oxide. *J. Phys. Chem. C* **2021**, *125*, 6073−6081.
(14) Mertens, F.; Mönkebüscher, D.; Parlak, U.; Boix-Constant, C.; Mañas-Valero, S.; Matzer, M.; Adhikari, R.; Bonanni, A.; Coronado, E.; Kalashnikova, A. M.; Bossini, D.; Cinchetti, M. Ultrafast Coherent THz Lattice Dynamics Coupled to Spins in the van der Waals Antiferromagnet $FePS_3$. *Adv. Mater.* **2023**, *35*, 2208355.
(15) Hou, D.; Qiu, Z.; Saitoh, E. Spin transport in antiferromagnetic insulators: progress and challenges. *NPG Asia Mater.* **2019**, *11*, 35.
(16) Radu, F.; Zabel, H. Exchange bias effect of ferro-/antiferromagnetic heterostructures. In *Magnetic Heterostructures: Advances and Perspectives in Spinstructures and Spintransport*; Springer: Berlin, Heidelberg, 2008; Vol. *227*, pp 97−184.
(17) Droghetti, A.; Thielen, P.; Rungger, I.; Haag, N.; Großmann, N.; Stöckl, J.; Stadtmüller, B.; Aeschlimann, M.; Sanvito, S.; Cinchetti, M. Dynamic spin filtering at the Co/Alq_3 interface mediated by weakly coupled second layer molecules. *Nat. Commun.* **2016**, *7*, 12668.
(18) Fourmental, C.; Le Laurent, L.; Repain, V.; Chacon, C.; Girard, Y.; Lagoute, J.; Rousset, S.; Coati, A.; Garreau, Y.; Resta, A.; Vlad, A.; Barreteau, C.; Smogunov, A.; Li, D.; Bellec, A. Evidence of a C_{60}/Co interface reconstruction and its influence on magnetic properties. *Phys. Rev. B* **2021**, *104*, 235413.
(19) Hassel, M.; Freund, H.-J. High resolution XPS study of a thin CoO (111) film grown on Co (0001). *Surf. Sci. Spectra* **1996**, *4*, 273−278.
(20) Biesinger, M. C.; Payne, B. P.; Grosvenor, A. P.; Lau, L. W.; Gerson, A. R.; Smart, R. S. C. Resolving surface chemical states in XPS analysis of first row transition metals, oxides and hydroxides: Cr, Mn, Fe, Co and Ni. *Appl. Surf. Sci.* **2011**, *257*, 2717−2730.
(21) Gruyters, M.; Riegel, D. Strong exchange bias by a single layer of independent antiferromagnetic grains: The CoO/Co model system. *Phys. Rev. B* **2000**, *63*, 052401.
(22) Radu, F.; Etzkorn, M.; Siebrecht, R.; Schmitte, T.; Westerholt, K.; Zabel, H. Interfacial domain formation during magnetization reversal in exchange-biased CoO/Co bilayers. *Phys. Rev. B* **2003**, *67*, 134409.
(23) Brems, S.; Buntinx, D.; Temst, K.; Van Haesendonck, C.; Radu, F.; Zabel, H. Reversing the training effect in exchange biased CoO/Co bilayers. *Phys. Rev. Lett.* **2005**, *95*, 157202.
(24) Kaeswurm, B.; O'Grady, K. The origin of athermal training in polycrystalline metallic exchange bias thin films. *Appl. Phys. Lett.* **2011**, *99*, 222508.
(25) Jenkins, S.; Chantrell, R. W.; Evans, R. F. Atomistic origin of the athermal training effect in granular IrMn/CoFe bilayers. *Phys. Rev. B* **2021**, *103*, 104419.
(26) Radu, F.; Etzkorn, M.; Schmitte, T.; Siebrecht, R.; Schreyer, A.; Westerholt, K.; Zabel, H. Asymmetric magnetization reversal on exchange biased CoO/Co bilayers. *J. Magn. Magn. Mater.* **2002**, *240*, 251−253.
(27) Suszka, A.; Idigoras, O.; Nikulina, E.; Chuvilin, A.; Berger, A. Crystallography-driven positive exchange bias in Co/CoO bilayers. *Phys. Rev. Lett.* **2012**, *109*, 177205.
(28) Gredig, T.; Krivorotov, I. N.; Eames, P.; Dahlberg, E. D. Unidirectional coercivity enhancement in exchange-biased Co/CoO. *Appl. Phys. Lett.* **2002**, *81*, 1270−1272.
(29) Dobrynin, A. N.; Warin, P.; Vorobiev, A.; Givord, D. On the origin of positive exchange bias and coercivity enhancement in proximity to the blocking temperature. *J. Magn. Magn. Mater.* **2021**, *520*, 166707.
(30) Stiles, M. D.; McMichael, R. D. Model for exchange bias in polycrystalline ferromagnet-antiferromagnet bilayers. *Phys. Rev. B* **1999**, *59*, 3722−3733.
(31) Dobrynin, A.; Givord, D. Exchange bias in a Co/CoO/Co trilayer with two different ferromagnetic-antiferromagnetic interfaces. *Phys. Rev. B* **2012**, *85*, 014413.
(32) Callsen, M.; Caciuc, V.; Kiselev, N.; Atodiresei, N.; Blügel, S. Magnetic hardening induced by nonmagnetic organic molecules. *Phys. Rev. Lett.* **2013**, *111*, 106805.
(33) Halder, A.; Bhandary, S.; O'Regan, D. D.; Sanvito, S.; Droghetti, A. Theoretical perspective on the modification of the magnetocrystalline anisotropy at molecule-cobalt interfaces. *Phys. Rev. Mater.* **2023**, *7*, 064409.
(34) Logemann, R.; Rudenko, A. N.; Katsnelson, M. I.; Kirilyuk, A. Exchange interactions in transition metal oxides: the role of oxygen spin polarization. *J. Phys.: Condens. Matter* **2017**, *29*, 335801.
(35) Pokhilko, P.; Zgid, D. Evaluation of Neel Temperatures from Fully Self-Consistent Broken- Symmetry GW and High-Temperature Expansion: Application to Cubic Transition-Metal Oxides. *J. Phys. Chem. Lett.* **2023**, *14*, 5777−5783.
(36) Fulcomer, E.; Charap, S. H. Thermal fluctuation aftereffect model for some systems with ferromagnetic-antiferromagnetic coupling. *J. Appl. Phys.* **1972**, *43*, 4190−4199.
(37) O'Grady, K.; Fernandez-Outon, L. E.; Vallejo-Fernandez, G. A new paradigm for exchange bias in polycrystalline thin films. *J. Magn. Magn. Mater.* **2010**, *322*, 883−899.
(38) Giannozzi, P.; Baroni, S.; Bonini, N.; Calandra, M.; Car, R.; Cavazzoni, C.; Ceresoli, D.; Chiarotti, G. L.; Cococcioni, M.; Dabo, I.; Dal Corso, A.; de Gironcoli, S.; Fabris, S.; Fratesi, G.; Gebauer, R.; Gerstmann, U.; Gougoussis, C.; Kokalj, A.; Lazzeri, M.; Martin-Samos, L.; Marzari, N.; Mauri, F.; Mazzarello, R.; Paolini, S.; Pasquarello, A.; Paulatto, L.; Sbraccia, C.; Scandolo, S.; Sclauzero, G.; Seitsonen, A. P.; Smogunov, A.; Umari, P.; Wentzcovitch, R. M. Quantum ESPRESSO: a modular and open-source software project for quantum simulations of materials. *J. Phys.: Condens. Matter* **2009**, *21*, 395502.
(39) Giannozzi, P.; Andreussi, O.; Brumme, T.; Bunau, O.; Buongiorno Nardelli, M.; Calandra, M.; Car, R.; Cavazzoni, C.; Ceresoli, D.; Cococcioni, M.; Colonna, N.; Carnimeo, I.; Dal Corso, A.; de Gironcoli, S.; Delugas, P.; DiStasio, R. A.; Ferretti, A.; Floris, A.; Fratesi, G.; Fugallo, G.; Gebauer, R.; Gerstmann, U.; Giustino, F.; Gorni, T.; Jia, J.; Kawamura, M.; Ko, H.-Y.; Kokalj, A.; Kucukbenli, E.; Lazzeri, M.; Marsili, M.; Marzari, N.; Mauri, F.; Nguyen, N. L.; Nguyen, H.-V.; Otero-de-la Roza, A.; Paulatto, L.; Ponce, S.; Rocca, D.; Sabatini, R.; Santra, B.; Schlipf, M.; Seitsonen, A. P.; Smogunov, A.; Timrov, I.; Thonhauser, T.; Umari, P.; Vast, N.; Wu, X.; Baroni, S. Advanced capabilities for materials modelling with Quantum ESPRESSO. *J. Phys.: Condens. Matter* **2017**, *29*, 465901.
(40) Lee, K.; Murray, E. D.; Kong, L.; Lundqvist, B. I.; Langreth, D. C. Higher-accuracy van der Waals density functional. *Phys. Rev. B* **2010**, *82*, 081101.
(41) Cooper, V. Van der Waals density functional: An appropriate exchange functional. *Phys. Rev. B* **2010**, *81*, 161104.
(42) Calloni, A.; Jagadeesh, M. S.; Bussetti, G.; Fratesi, G.; Achilli, S.; Picone, A.; Lodesani, A.; Brambilla, A.; Goletti, C.; Ciccacci, F.; Duò, L.; Finazzi, M.; Goldoni, A.; Verdini, A.; Floreano, L. Cobalt atoms drive the anchoring of Co-TPP molecules to the oxygen passivated Fe(001) surface. *Appl. Surf. Sci.* **2020**, *505*, 144213.

https://doi.org/10.1021/acsaelm.3c01599
ACS Appl. Electron. Mater. 2024, 6, 3138−3146

(43) Dal Corso, A. Pseudopotentials periodic table: from H to Pu. *Comput. Mater. Sci.* **2014**, *95*, 337−350.

https://doi.org/10.1021/acsaelm.3c01599
ACS Appl. Electron. Mater. 2024, 6, 3138−3146